An Improved Technique for Computing the Horizontal Pressure-Gradient Force at the Earth's Surface

WAYNE E. SANGSTER

National Weather Service Central Region, Scientific Services Division, Kansas City, MO 64106

(Manuscript received 4 April 1986, in final form 22 December 1986)

ABSTRACT

On conventional surface analyses, sea level isobars allow a forecaster to compute the horizontal pressure-gradient force at sea level, which for much of the world is fairly close to the earth's surface. However, over elevated terrain the procedures invoked in reducing the observed station pressures to sea level can give results that are markedly different from those obtained directly from surface data, as shown in an earlier paper by the author. This paper represents an extension of that work. A revised variable reference atmosphere is developed and used as an aid in computing the horizontal pressure-gradient force on a smoothed terrain approximating the earth's surface. Surface observations are input to the procedure, and surface geostrophic winds, or alternatively, stream and potential functions of the surface geostrophic wind, are output.

The methods described herein are currently in operational use at the National Meteorological Center. Charts are shown for summer situations over the Great Plains when and where they have especial utility, as well as for a winter case where the reduction-to-sea level process led to very strong gradients over elevated terrain on sea level pressure charts.

1. Introduction and historical perspectives

A basic variable measured by the weather services of the world is the pressure at the surface of the earth, known as the *station* pressure. If one were to draw a chart with isobars of station pressure, the result would look more like a terrain contour map than a useful weather map, unless the terrain is level. This, of course, is due to the fact that atmospheric pressure is a strong function of elevation.

The conventional way of producing charts which are more useful is to reduce station pressures to sea level. The idea here supposedly is that the pressure gradients thus implied would tell something about the horizontal pressure-gradient force (HPGF) at the earth's surface. It is obvious, however, that if the fictitious layer between the earth's surface and sea level is by assumption "baroclinic," the sea level HPGF would not be the same as that at the earth's surface. Much of the time the assumed baroclinity is not large and at many places the terrain is not greatly elevated, so the procedure works fairly well. At other times and places it does *not* work well.

Harrison (1957, 1970) and Shuman (1957) recognized this problem and devised methods of computing functions that could be used to approximate the HPGF at the earth's surface instead of at sea level. In a paper by the author (Sangster, 1960, hereafter referred to as WES), it was shown that a direct computation of the HPGF at the earth's surface could be made by using station pressures and surface virtual temperatures. In WES the procedure was to use the altimeter correction system of Bellamy (1945), a smoothed terrain, and finite difference methods to produce stream and potential functions of the surface geostrophic wind. This paper documents revisions to some of the methods used in WES and also provides case studies which highlight the advantages of looking at the surface HPGF directly, rather than deducing something about it from the sea level charts.

Specifically, this paper reformulates the method of calculation of the "reference" atmosphere described in WES and presents a new method of specifying boundary conditions for the elliptic partial differential equations involved. These methods are currently in operational use by the National Weather Service (NWS) to produce a "surface geostrophic wind" (SGW) chart. This chart has gained wide acceptance throughout the NWS and other weather services.

Operational use of the SGW chart began in the late 1960s at the National Severe Storms Forecast Center in Kansas City, Missouri in the form of internally used products. Crude alphanumeric transmission of the data to other offices began in April 1974. Graphic products are now currently transmitted eight times daily over the NWS communications network. These charts have wind shafts and barbs of the SGW at grid points and isopleths of the surface geostrophic relative vorticity.

2. Computation of the temperature anomaly of the reference atmosphere

a. The altimeter correction system

The altimeter correction system of Bellamy (1945) is used here and in this system the hydrostatic equation takes on two very simple forms:

$$\frac{\partial D}{\partial Z_p} = S^* \tag{1}$$

or

$$\frac{\partial D}{\partial Z} = \frac{S^*}{1+S^*}. \tag{2}$$

Here, $D \equiv Z - Z_p$ and $S^* \equiv (T^* - T_p)/T_p$, where D is the altimeter correction, Z is geopotential height, Z_p is pressure altitude, S^* is the specific virtual temperature anomaly, T^* is the virtual temperature, and T_p is the temperature in the standard atmosphere used to compute Z_p. The D field reflects topographic features much less than does the station pressure field, since the standard atmosphere variation of pressure with height is removed.

As in WES the slope of an isobaric surface in the "sigma" vertical coordinate system of Phillips (1957) is given by

$$\nabla_p Z = \nabla_p D = \nabla D - S^* \nabla Z_p \tag{3}$$

where the subscript p implies differentiation in isobaric coordinates while differentiation in the sigma system carried no subscripts.

b. Definition of the new reference atmosphere

As an additional refinement, a variable reference atmosphere is introduced by allowing its specific virtual temperature anomaly (S_r) at a given time to be variable with x and y, but independent of Z_p. Integration of the hydrostatic equation (1) from some arbitrary constant base level $\hat{Z}_p$ to Z_p gives

$$D_r = S_r(Z_p - \hat{Z}_p) \tag{4}$$

where D_r is the D value in the reference atmosphere and is taken to be zero at the base level.

If Z_r is geopotential height in the reference atmosphere, (4) shows that

$$Z_r = Z_p + D_r = Z_p + S_r(Z_p - \hat{Z}_p). \tag{5}$$

Defining the altimeter correction with respect to the new reference atmosphere by $D' = Z - Z_r$, we find from (5) that

$$D' = D - S_r(Z_p - \hat{Z}_p) \tag{6}$$

where D' is a new surrogate station pressure variable replacing D, and can be thought of as a D value reduced to the base level Z_p by using the temperature S_r. It is of interest to note that

$$\frac{\partial D'}{\partial Z_p} = S^* - S_r. \tag{7}$$

Thus, the dependence of D' on Z_p is weak as long as the difference between S^* and S_r is small. Under these conditons, orographic features show up to a lesser extent in the D' field than in the D field.

At this point, we are ready to derive a defining equation for the field of S_r. We do this by requiring that D' be the approximate geostrophic streamfunction, the Laplacian of which yields the geostrophic relative vorticity on a sigma surface, neglecting the variation of the Coriolis parameter (f) and the scale factor (m) with latitude. This gives from (3), since we assume $\nabla^2 D' = \nabla \cdot \nabla_p D$,

$$\nabla^2 D' = \nabla^2 D - \nabla \cdot (S^* \nabla Z_p). \tag{8}$$

From (6) we find that

$$\nabla^2 D' = \nabla^2 D - \nabla^2 [S_r(Z_p - \hat{Z}_p)]. \tag{9}$$

An equation for S_r is found from (8) and (9), which is

$$\nabla^2 [S_r(Z_p - \hat{Z}_p)] = \nabla \cdot (S^* \nabla Z_p) \tag{10}$$

Since D at grid points is not yet known, neither is Z_p, so we make the approximation that $Z_p = Z$ in (10). Since D is an order of magnitude smaller than Z this causes no great problems, especially since S_r need not be known exactly. The $\hat{Z}_p$ has to be chosen so that $(Z_p - \hat{Z}_p)$ is always positive in order to avoid division by zero in the relaxation procedure, and $\hat{Z}_p$ is chosen by trial and error to give a smooth S_r field without making $(Z - \hat{Z}_p)$ excessively large. In this study a value of -150 m was used. Equation (10) was solved for S_r by relaxation methods under the condition that the normal derivative of S_r vanish on the boundary. Then S_r is interpolated to stations, D' is computed at stations from (6) and then analyzed to grid points. The value of D then can be computed at grid points from D' and S_r from (6), giving the means to compute Z_p at grid points ($Z_p = Z - D$). Both analysis operations (for S^* and D') were performed using the Cressman (1959) technique on a grid with a 174 km (at 45° latitude) mesh size.

Finally, (3) can be rewritten as

$$\nabla_p Z = \nabla D' - (S^* - S_r)\nabla Z_p + (Z_p - \hat{Z}_p)\nabla S_r. \tag{11}$$

This equation has the advantage that both $|S^* - S_r|$ and $|S_r|$ tend to be minimized, since S_r is a smoothed field of S^*. Exactly how S_r comes out is determined by the selection of $\hat{Z}_p$. By itself D' gives most of the HPGF under common synoptic situations, as examples to be shown will illustrate. This is not true of D and certainly is not true of station pressures over sloping terrain.

3. Geostrophic stream and potential functions

The geostrophic "stream" (H) and "potential" (G) functions are defined in WES so that the geostrophic wind is given by

$$\mathbf{V}g = \frac{-g}{f}(\nabla H \times \mathbf{k} + \nabla G). \tag{12}$$

The reader is referred to WES for details of the computations to follow since this work followed the earlier work closely.

Since we are in the sigma system there is a divergence of the geostrophic wind and it follows that a potential function is needed in (12). While this divergent contribution to the geostrophic flow in isobaric coordinates is zero, it can have a significant magnitude in this sigma-coordinate system (see WES for a case where the G field contributes greatly to the geostrophic wind). This does not mean, however, that one can deduce areas of clouds and precipitation by looking at the G field. The continuity equation in the sigma system is also different from that in the isobaric system. Obviously, the physical fact that the vertical velocity does not change much in the vertical if the winds are geostrophic remains unaltered by simply using a different coordinate system.

Since $V_g = -(g/f)\nabla_p Z \times \mathbf{k}$ we find from (11) and (12) that

$$\nabla^2 H = \nabla^2 D' - \nabla \cdot [(S^* - S_r)\nabla Z_p - (Z_p - \hat{Z}_p)\nabla S_r] \quad (13)$$

and

$$\nabla^2 G = J(Z_p, S^*) \quad (14)$$

where $J(Z_p, S^*)$ is the Jacobian determinant of Z_p and S^* with respect to x and y. The variable reference atmosphere does not affect the equation for G.

Then (13) is solved for H, using the condition that

$$H = D' - S_r \hat{Z}_p \quad (15)$$

on the boundary. This specification is tantamount to specifying that $H = D - S_r Z_p$: i.e., the streamfunction on the boundary is the D value reduced to the 1013.25 mb surface ($Z_p = 0$ in the standard atmosphere) by using the reference atmosphere temperature anomaly as the column temperature.

Here G is obtained from (14) by using the component equation relationships for the tangential derivative of G in terms of the normal derivative of H, S^*, S_r and Z_p to integrate around the boundary, starting in the lower left corner with the value of zero (as described in WES).

4. Use of a smoothed reference surface

Since the partial differential equations in H and G were solved using finite differences, a smoothed topography is used as in numerical weather prediction models. The one used herein (Fig. 1) was constructed from station elevations rather than from detailed terrain heights. Since stations tend to be in valleys, this

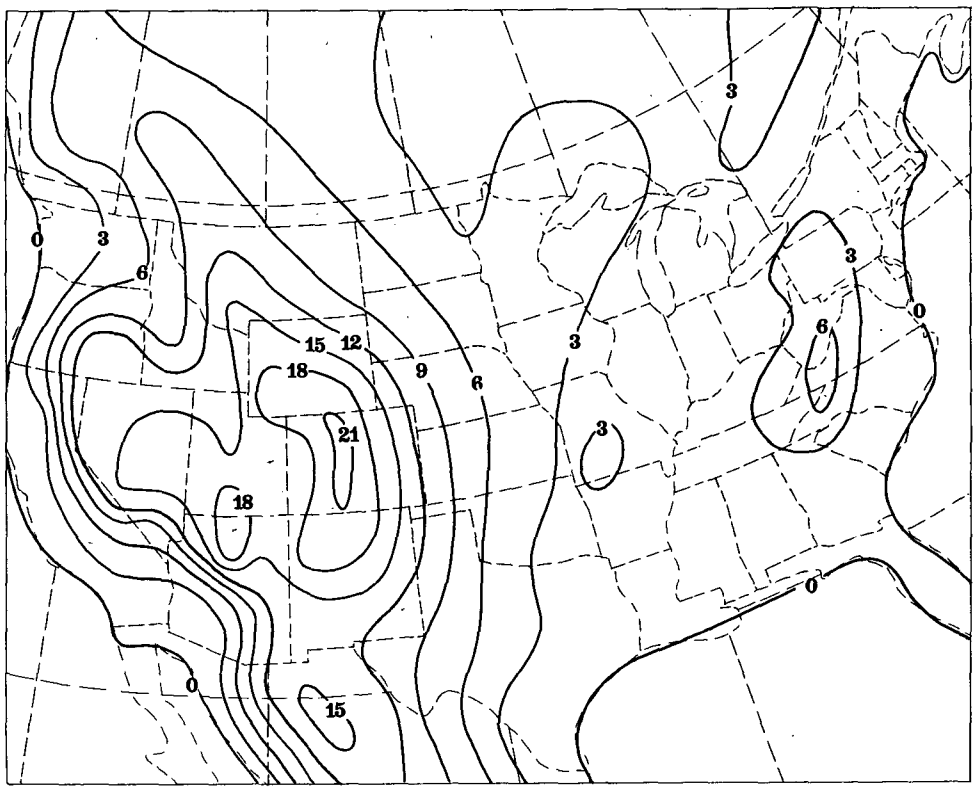

FIG. 1. Smoothed terrain used in the computations. Elevations above sea level are in hectometers with a contour interval of 3 hm. The smoothing was done to fit *station* elevations rather than the actual terrain elevations.

gives a generally lower terrain than was used in WES and tends to minimize the magnitude of the reduction procedure.

Values of D and S^* are reduced to this terrain under the assumption that T^* is a constant between the actual ground level and the smoothed terrain. The derivation of the equation for the reduced D value is given in the Appendix.

5. Effects of the "plateau correction" used in reducing station pressures to sea level

For stations in the United States above 305 m elevation there is implicitly included in the operational reduction-to-sea level procedure the effect of the "plateau correction" conceived by Ferrell (1886). The process is described in great detail by Harrison (1963), but we will say only enough here to help understand the comparisons to be shown in the next section where its presence is apparent.

Briefly, we can simply say that the plateau correction is a function of the difference between the surface temperature argument used in the reduction algorithm (the average of the current temperature with that 12 hours previous) and the annual normal surface temperature for the station. The effect of this "correction" is to make sea level pressures higher than they would otherwise be in the summer over a plateau and lower than they would otherwise be in the winter. The hotter the summer temperatures are, the greater the effect, and likewise in the opposite sense for extreme winter temperatures.

We made an attempt to quantify the effect of the plateau correction under extreme conditions, and without going through all the details of that experiment, it suffices to say that the plateau correction contributes to a *north* geostrophic wind component at sea level in the summer over the Great Plains, and a *south* geostrophic wind component there in the winter. The magnitudes of this component are around 10 m s^{-1}, certainly large enough to be important.

6. Case studies

The author's original efforts at devising a better method of computing the HPGF at the earth's surface were prompted by his interest in boundary layer wind maxima (BLWM) (Blackadar, 1957) over the Great Plains. This interest was in turn due to efforts to understand the causative mechanisms for the nocturnal thunderstorms prevalent in the north central United States during the warm season. Through the years of looking at the SGW charts it has become apparent that they are of particular value over the Great Plains, which we hope to show. They have proved to be of some benefit in forecasting nocturnal thunderstorms (Sangster, 1979).

From a publication of the National Climatic Data Center (U.S. Department of Commerce, 1983), we tabulated the ten locations in the contiguous 48 states in their listing which had the highest average wind speed for the summer months (June, July and August). Three of the top ten were either mountainous (Mt. Washington, NH) or coastal (Blue Hill, MA and San Francisco International Airport, CA). The other seven were in an area bounded by 32° and 40°N, 97° and 102°W on the Great Plains. The locations of these stations are shown in Fig. 2. While part of this windiness may be due to the lack of terrain features, we will show that there are frequently very strong southerly SGWs during the day over the area. BLWMs are also prevalent in this area (Bonner, 1968).

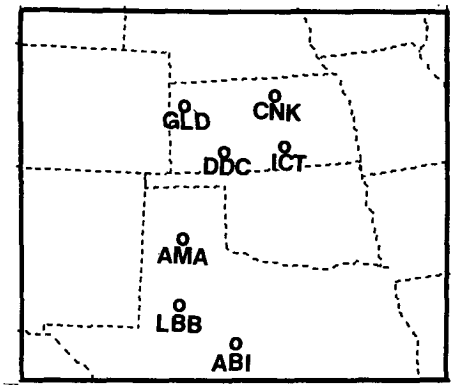

FIG. 2. The seven Great Plains stations of the top ten in the United States having the highest average wind speed for the summer. They are Goodland, KS (GLD), Concordia, KS (CNK), Dodge City, KS (DDC), Wichita, KS (ICT), Amarillo, TX (AMA), Lubbock, TX (LBB), and Abilene, TX (ABI).

The first sets of maps focus on this area in summer. SGW barbs and shafts (rather than geostrophic stream and potential functions) are shown overlaid with a computer analysis of the sea level pressure (SLP) isobars. These charts are available eight times per day on the NWS communications system.

a. The case of 9 to 11 July 1986

Figure 3 has SGW charts with SLP isobars for three times of the day for three consecutive days. The times chosen are 1200, 2100 and 0000 UTC.

Figure 3a (for 1200 UTC) shows two SLP lows over Kansas with a SLP high over northwest New Mexico. The SGW plots agree fairly well with the SLP isobars over the Great Plains. By 2100 UTC (Fig. 3d) there is only one SLP low in southwest Kansas. Obviously, the sea level geostrophic wind (SLGW) at the low center is calm. However, the plot in southwest Kansas indicates a SGW of about 170° at 15 m s^{-1}. Farther south over the Texas panhandle the SGWs are nearly perpendicular to the SLP isobars. By 0000 UTC (Fig. 3g) the SGW at the SLP low center in western Kansas had decreased to 13 m s^{-1}, as had the SGWs over the Texas Panhandle. On this day a considerable thermal wind was implied by the SLP over the high country.

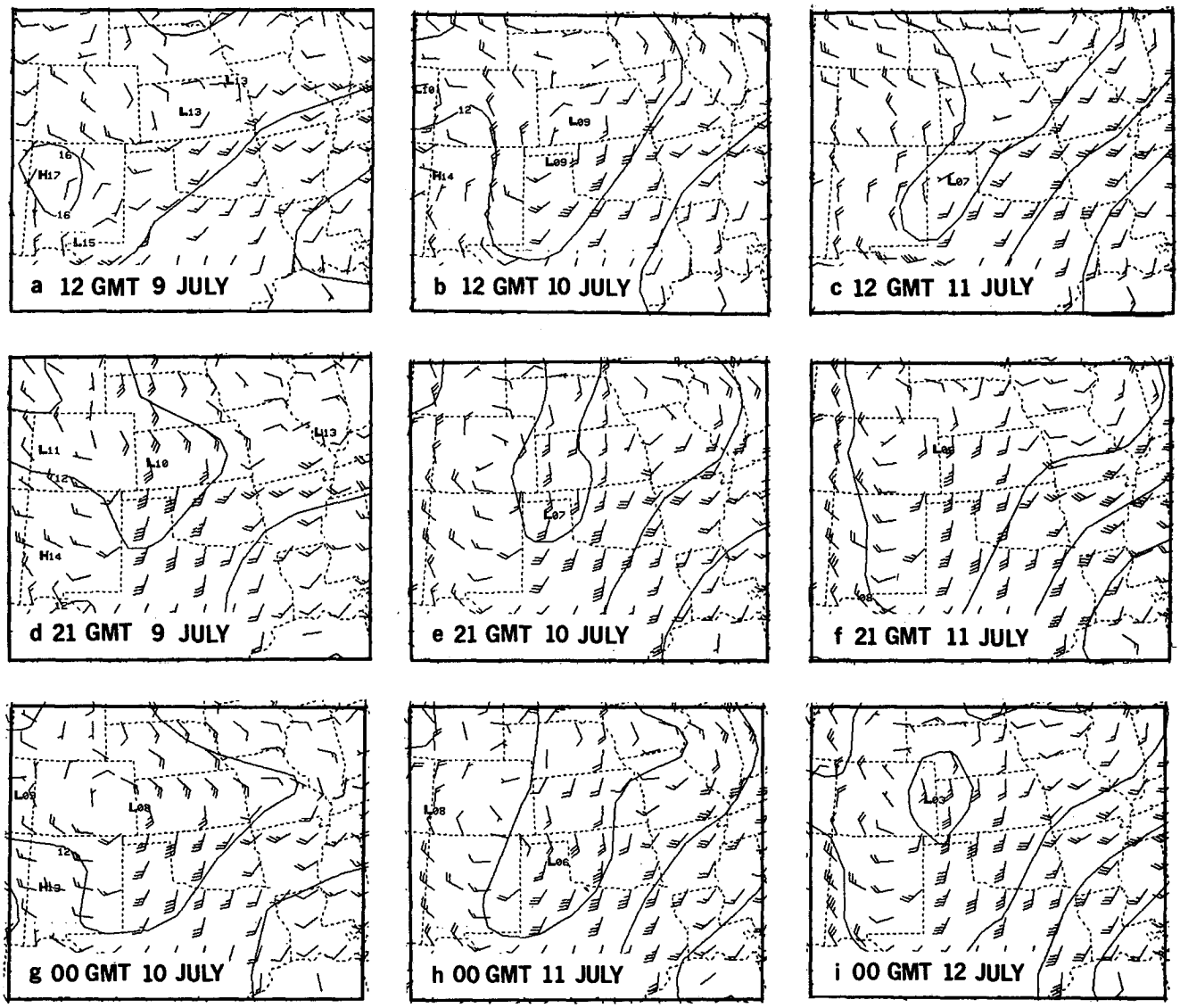

FIG. 3. Surface geostrophic winds for (a) 1200 UTC 9 July, (b) 1200 UTC 10 July, (c) 1200 UTC 11 July, (d) 2100 UTC 9 July, (e) 2100 UTC 10 July, (f) 2100 UTC 11 July, (g) 0000 UTC 10 July, (h) 0000 UTC 11 July, and (i) 0000 UTC 12 July 1986. A full barb is 5 m s^{-1} and a flag is 25 m s^{-1}. The isopleths are of sea level pressure at 4 mb intervals with the leading "10" omitted.

By 1200 UTC of the next morning (Fig. 3b), the agreement between the SGW plots and the SLP isobars was good around the twin SLP lows in southwest Kansas and the Texas Panhandle. As happened the previous day, by 2100 UTC chart (Fig. 3e) there was a SGW of 15 m s^{-1} "blowing through" the SLP low center in the Texas Panhandle. In extreme southeast Colorado there is a *south* SGW to the west-northwest of the SLP low, where there should be northeast SLGWs. By 0000 UTC (Fig. 3h), the SGW speeds had diminished some as they did the previous day.

As for the previous two days, the 1200 UTC chart for 11 July (Fig. 3c), there is fairly good agreement between the SGW and the SLGW around the SLP low in the Texas Panhandle. By 2100 UTC (Fig. 3f), there were SGWs of 18 m s^{-1} pointing toward the SLP low in northwest Kansas. There is a south SGW to the west of this low. The last map (Fig. 3i) also shows a south SGW west of the SLP low.

The three-day series displays the diurnal variation of the SGW over the Plains as described by Sangster (1967) and confirmed by Bonner and Paegle (1970). The 1200 UTC charts do not show as much difference between the SGW and the SLGW as do the charts during the hot part of the day at 2100 and 0000 UTC. The lack of a diurnal variation in the SLGW is due to the averaging used to get the temperature reduction argument previously described (the current temperature and that 12 hours previous). The reason the oscillation of the SGW north–south component does not average

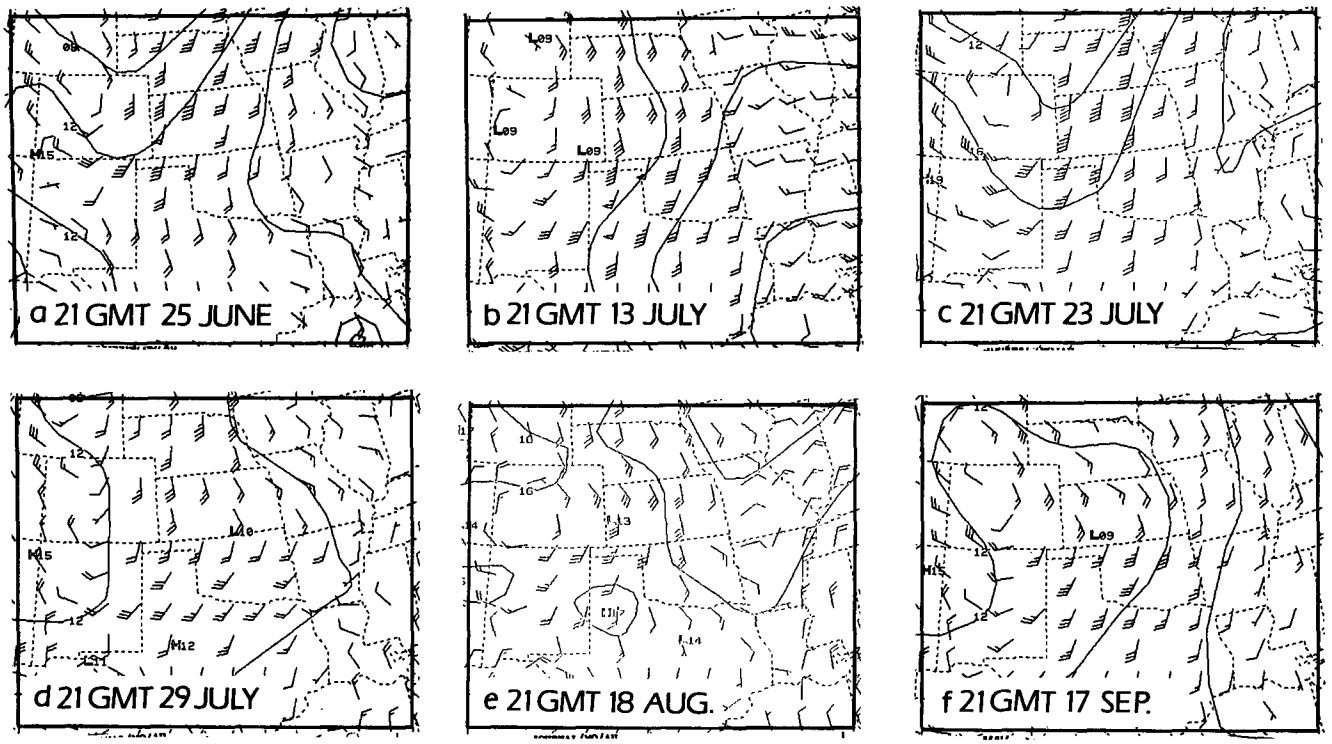

FIG. 4. As in Fig. 3 except for (a) 2100 UTC 25 June, (b) 2100 UTC 13 July, (c) 2100 UTC 23 July, (d) 2100 UTC 29 July, (e) 2100 UTC 18 August, and (f) 2100 UTC 17 September, all in 1986.

about the same as the SLGW is due to the effects of the plateau correction which we have previously estimated to have a magnitude of about 10 m s^{-1} directed out of the north in hot summer conditions.

b. Some selected 2100 UTC cases

Of the eight charts produced daily, the 2100 UTC chart consistently has the strongest SGWs under typical southerly flow in the warm season over the central High Plains. The three day period in the last case study was typical in this respect, as operational use has shown through the years. In this section, we will present six 2100 UTC charts for other days during the warm season of 1986 to demonstrate that the 9–11 July case was not a "flash in the pan."

(i) 25 June 1986 (Fig. 4a). Near the SLP trough line in eastern Colorado there is a south SGW of 18 m s^{-1}, an obvious difference. At the trough line the westerly SLGW is about 8 m s^{-1}. Over extreme western Kansas there is a southerly SGW of 26 m s^{-1} compared with a SLGW from the southwest at about 13 m s^{-1}. Note the south-southeasterly SGWs in extreme eastern Wyoming, which do not agree at all with the implied SLGWs in direction, considering the fact that there is a SLP low in southern North Dakota.

(ii) 13 July 1986 (Fig. 4b). The 1009 mb SLP low in southeast Colorado has a 13 m s^{-1} SGW "blowing through" it. Over the Texas Panhandle, there is a 28 m s^{-1} SGW from the south-southwest in comparison with a 10 m s^{-1} SLGW, as estimated from the central SLP of 1009 mb and the location of the 1012 mb isobar.

(iii) 23 July 1986 (Fig. 4c). SGWs up to 23 m s^{-1} are present over the Oklahoma Panhandle and extreme western Kansas with directions which nearly parallel the trough axis on the SLP isobars.

(iv) 29 July 1986 (Fig. 4d). This day was notable because of the extremely hot surface temperatures over the central Great Plains. Dodge City, Kansas and Oklahoma City, Oklahoma both reported 42.8°C, which tied the all-time record for any month at Dodge City. Under these conditions, the plateau correction was influencing the SLPs to the extreme. There was a 1010-mb low on the SLP analysis along the Kansas–Oklahoma border, but southerly SGWs of 12 to 15 m s^{-1} to the west of the low center. The SGW was "blowing through" the 1012-mb high in west Texas on the SLP chart.

(v) 18 August 1986 (Fig. 4e). Here again a 15 m s^{-1} SGW was "blowing through" the SLP low in western Kansas, as was a 8 m s^{-1} SGW through the SLP high in northwest Texas.

(vi) 17 September 1986 (Fig. 4f). This is another case similar to 29 July (d above) in that there are southerly SGWs to the west of the SLP low in southwest

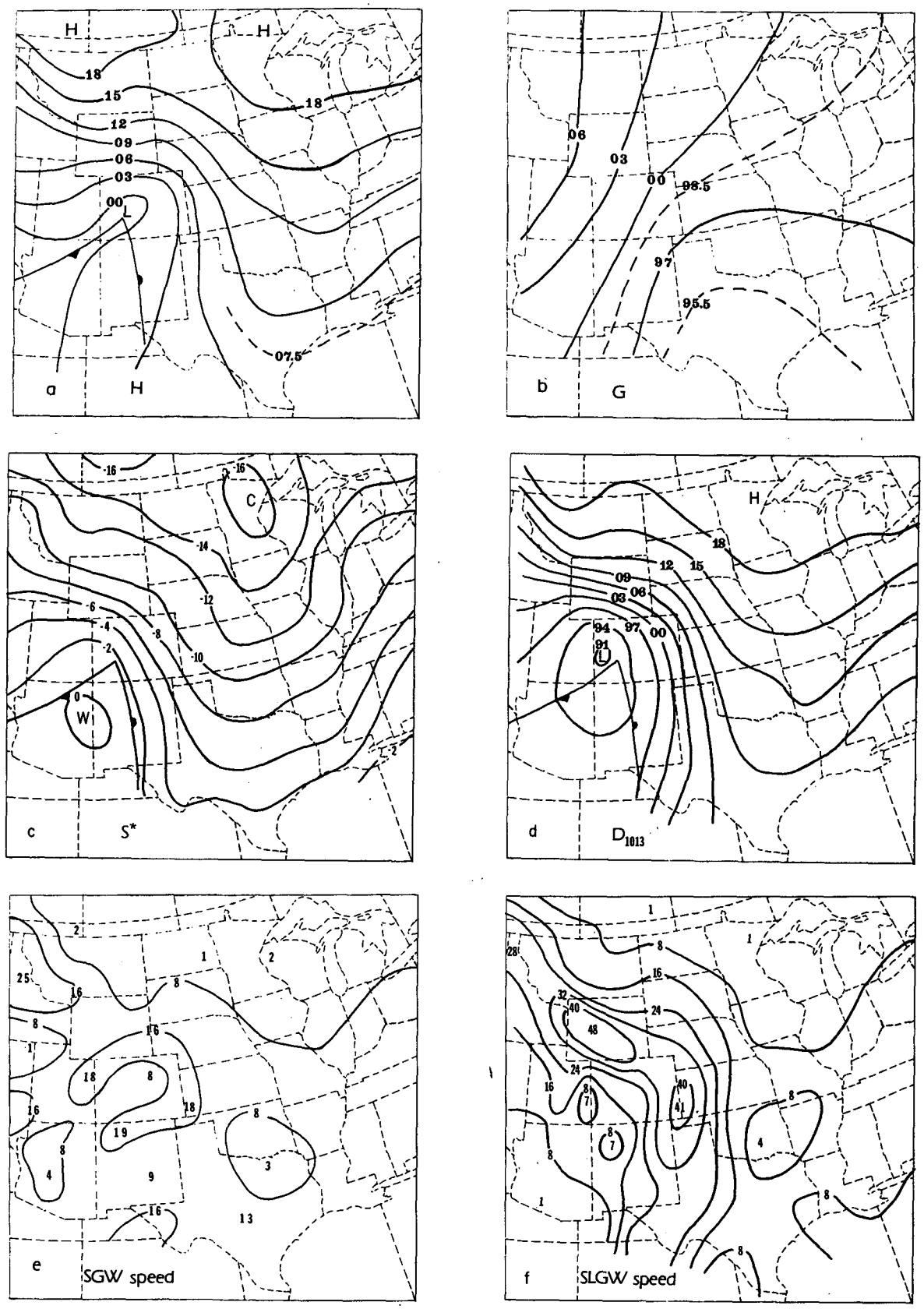

FIG. 5. Charts for 1200 UTC 20 December 1983: (a) surface geostrophic stream function (H) at 3 dam intervals, (b) surface geostrophic potential function (G) at 3 dam intervals, (c) surface S^* value at 2 percent intervals, (d) D_{1013} at 3 dam intervals, (e) isotachs of surface geostrophic wind speeds at 8 m s^{-1} intervals, and (f) isotachs of sea level geostrophic wind speed at 8 m s^{-1} intervals.

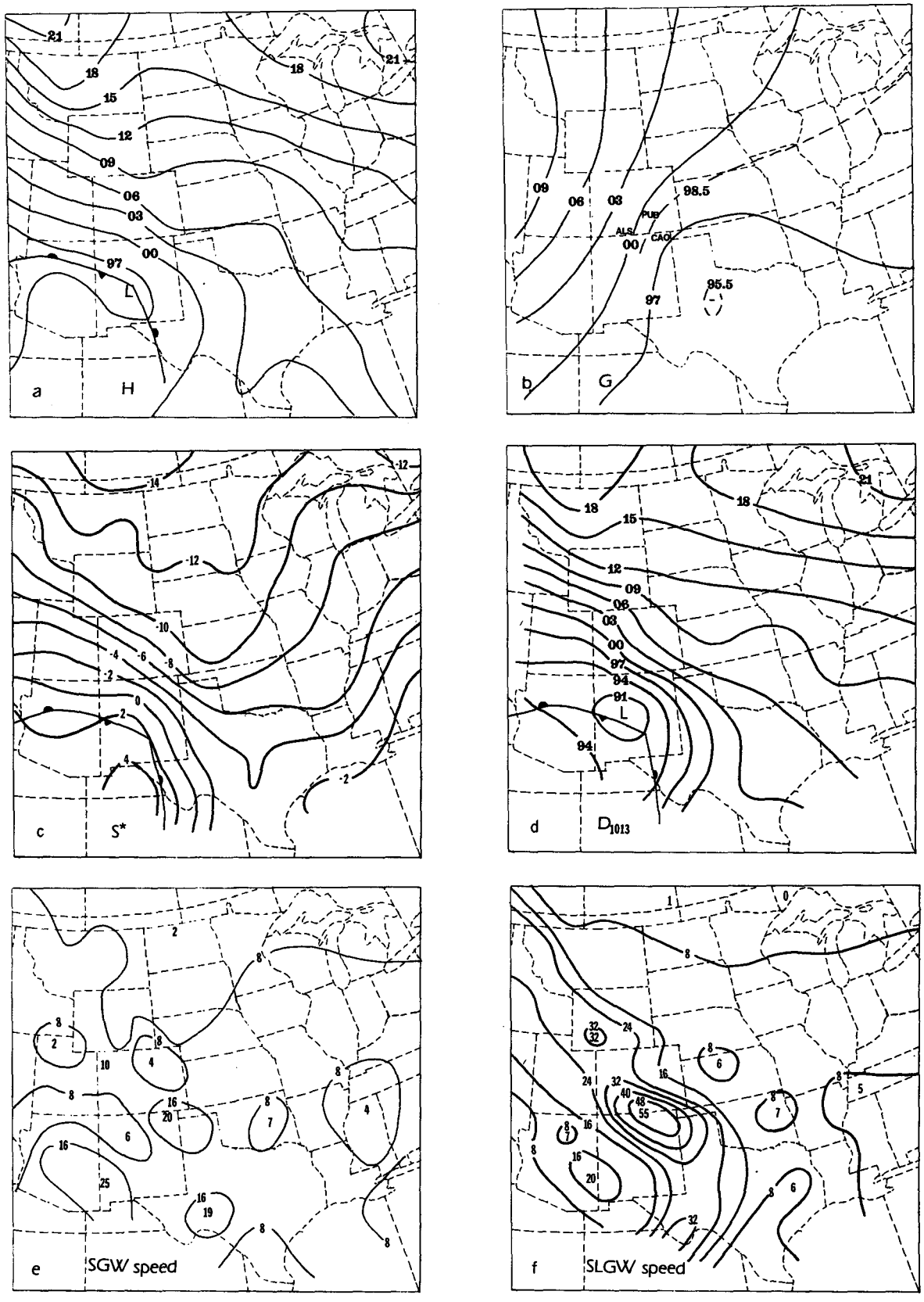

FIG. 6. As in Fig. 5 except for 0000 UTC 21 December 1983.

Kansas. A southwest SGW of 8 m s^{-1} is located in a SLP col over the New Mexico–Texas border.

All of the above indicates that over the Great Plains in summer large differences between the SLGW and the SGW are common. The SGWs during the day help explain the windiness of this area noted earlier. BLWMs are common at stations like Dodge City and Amarillo during the night and the strong SGWs during the previous day are an important factor in their development as shown by Bonner and Paegle (1970).

c. *An extreme winter case: 20–21 December 1983*

In the preceding section, we have presented charts as they are transmitted to field forecasters in the NWS and elsewhere. In this section, an alternative form of display is used—namely, that of the geostrophic stream and potential functions, as was done in WES. It is likely that both forms of display could eventually be used operationally, depending upon the application.

So that we can compare charts which have the same units, instead of SLP charts we show charts of D_{1013}, defined to be the D value reduced to the 1013.25 mb surface (sea level in the standard atmosphere). Thus, we may write

$$D_{1013} = D_{sl} - S^*_{col}(Z_{psl} - Z_{p1013}) \tag{16}$$

where D_{sl} is the D value at sea level and S^*_{col} is the column temperature which for simplicity we take to be the same as that at the surface of the earth. This assumes a standard atmosphere lapse rate in the subterranean column. Also Z_{psl} and Z_{p1013} are the pressure altitudes at sea level and 1013.25, respectively.

Now we note that $D_{sl} = Z_{sl} - Z_{psl} = -Z_{psl}$, since the geopotential height at sea level is zero. Also, by definition Z_{p1013} is zero. So (16) becomes

$$D_{1013} = -(1 + S^*_{col})Z_{psl} \tag{17}$$

where Z_{psl} is obtained from the SLP using the properties of the standard atmosphere.

On 20–21 December 1983, very cold air had pushed quite far south over the central part of the United States. In that area it was one of the colder periods during a very cold December—the coldest in at least 53 years for the United States as a whole (Quiroz, 1984). The charts to be shown then represent an uncommon situation, deliberately chosen to highlight the differences between the SLGW and the SGW.

Six-panel figures for 1200 UTC 20 December and 0000 UTC 21 December 1983 are shown in Figs. 5 and 6. Charts are given for the geostrophic stream (H) and potential functions (G), surface specific virtual temperature anomaly (S^*), D_{1013}, and geostrophic wind isotachs for both the SGW and SLGW.

On Fig. 5c, an axis of cold air extends from near Duluth, Minnesota through Kansas City, Missouri and to the southern tip of Texas. The thermal gradient is strong over the elevated terrain of Wyoming, Colorado, and eastern New Mexico. According to the reduction process for SLPs (D_{1013}), the isobars (contours) should tend to parallel the isotherms, which is indeed what is found in Fig. 5d, in the vicinity of the thermal packing.

Maximum SLGW wind speeds as high as 41 m s^{-1} just north of the Oklahoma Panhandle and 48 m s^{-1} in western Wyoming result from the contour packing in the D_{1013} field. In contrast, H and G together produce maximum speeds of 18 m s^{-1} (see Fig. 5e) in different places from what is indicated by the D_{1013} chart. As a point of comparison, the speed in western Wyoming is only about 12 m s^{-1}, one quarter of that given by the SLP chart.

Figure 5b shows that the contribution of the potential function is not negligible. At some locations (e.g., central Colorado), the potential function gives a component in almost the exact opposite direction from that given by the stream function. Since the partitioning of the geostrophic wind between the two functions is partly determined by the boundary conditions and the domain over which the computation is done, it is possible to minimize the contribution of the potential function with different boundary conditions (see WES). It is never possible, however, to reduce its contribution to zero.

The D_{1013} 41 m s^{-1} SLGW maximum just to the north of the Oklahoma Panhandle in Fig. 5f can be compared with the winds in the boundary layer of 9 m s^{-1} at Dodge City, Kansas and 15 m s^{-1} at Amarillo, Texas at this time. The maximum SGW in southwest Kansas was 18 m s^{-1} at Amarillo the value was 13 m s^{-1}.

Turning to the charts 12 hours later, a SLGW of 55 m s^{-1} on the Colorado–New Mexico border is the highlight of the D_{1013} chart (Fig. 6f). In contrast, the SGW gives speeds only of 10 to 12 m s^{-1} in this area (Fig. 6e). The packing of the isotherms in Fig. 6c is greatest in this area, so a large subterranean thermal wind in the SLP package is the cause of this difference.

Figure 6b is noteworthy from the standpoint that the contribution of the potential function field (G) is quite large over the southern mountain states. In fact, over Colorado the spacing is almost as tight as on the streamfunction chart (Fig. 6a). Another feature of the G chart which is of interest is a "sink" (indicated by the minus sign) over north-central Texas. This gives a north to northwest flow component over the Central Plains which tends to drive the cold air south. From (14) we find that this sort of an arrangement will occur if the isotherms and the terrain contours cross at a large angle (as they do with an east–west front across the Great Plains). This effect tends to force cold air to move south behind a cold front, even though the H field does not give much of a component normal to the front. So, as was noted in WES, Arctic plunges across the High Plains are not really as ageostrophic as one would believe by looking at SLP charts. Other

TABLE 1. Surface winds at the stations indicated.

0000 UTC 21 December 1983 (See Fig. 6b for locations)	
Clayton, New Mexico (CAO)	020°/6 m s^{-1}
Alamosa, Colorado (ALS)	200°/5 m s^{-1}
Pueblo, Colorado (PUB)	120°/4 m s^{-1}

effects such as rapid pressure changes and friction, of course, lead to ageostrophic motion in these situations.

No upper air stations exist close enough to make a valid comparison with the 55 m s^{-1} maximum in the SLGW (Fig. 6f), but the surface winds at three stations in the area are given in Table 1. The wind at Alamosa is subject to local effects since the station is surrounded by mountains, but the other sites have nothing but plains to the east so local effects should be minimized. The SGW speeds (Fig. 6e) are more in line with the Clayton and Pueblo surface wind speeds than the SLGW charts.

7. Some effects of introducing a variable reference atmosphere

Charts of S^*, S_r, D' and D are shown in Fig. 7 and for one time during the December 1983 case discussed above. We will briefly point out the highlights of these charts to illustrate the performance of the reference atmosphere.

Comparing Fig. 7a with Fig. 7b we see that the gradients of S_r are much weaker than those of S^* over

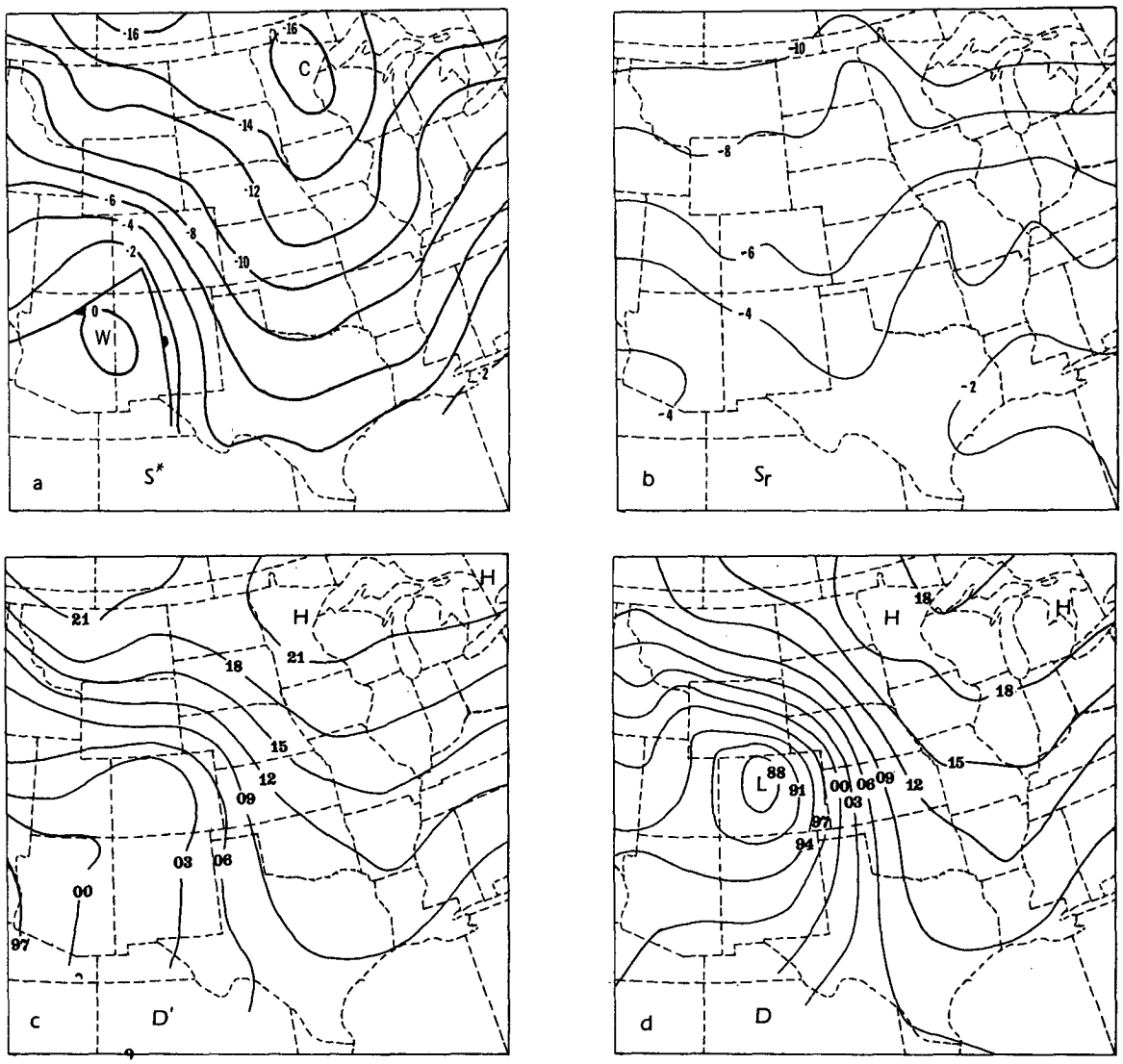

FIG. 7. Charts for 1200 UTC 20 December 1983: (a) surface S^* value at 2 percent intervals, (b) computed S_r value at 2 percent intervals, (c) surface D' values at 3 dam intervals, and (d) surface D values at 3 dam intervals.

the mountains of the west. The D' pattern (Fig. 7c) looks very similar to that of H in Fig. 5a. As (13) shows H differs from D' for three reasons: 1) the difference between S^* and S_r over sloping terrain, 2) the gradient of S_r over elevated terrain, and 3) the lateral boundary conditions. Apparently these effects are not great.

The D field has much lower values over the high terrain than does D'. This is to be expected since the hydrostatic relationship (1) says that D values decrease with pressure altitude under colder-than-standard conditions, whereas (7) says that it is only the difference between S^* and S_r which influences the D' variation with pressure altitude. Since there is a one-to-one correspondence between altimeter setting and D value, this fact affects the use of the altimeter setting as a means of portraying the surface pressure field as practiced by some (e.g., Magor, 1958). Altimeter settings will work fairly well if temperatures are near standard, but since such conditions are the exception rather than the rule, this practice should not be condoned.

In the procedures described in this paper, the only time a "pressure" variable is analyzed from stations to grid points is in the D' analysis. If D were to be directly analyzed one would expect an inferior product because both topography and pressure effects would be mixed together. We believe that it is better to analyze D' and then compute D (which is necessary to get Z_p).

8. Conclusions

From the foregoing, it is quite clear that, in the age of computers, sea level pressures are inadequate to describe the geostrophic wind at some times and places. The methods used here could provide a basis for more accurate specification of the initial conditions at and near the ground with regard to the pressure field for use in numerical prediction models. It makes no sense to have sophisticated models of the atmosphere running on large and fast computers, only to degrade the procedures by using pressures reduced to sea level or 1000 mb as input and/or output. Even if analyses are made directly in sigma coordinates, care must be taken to insure that errors do not arise because of the tendency of the two terms in the expression for the HPGF to be large and of opposite sign. While this paper deals only with observed data, it is obvious that the same ideas could be applied to forecast data quite easily.

The method of display used in sections 6a and 6b has proven to be quite useful for short-term forecasting. For model output the geostrophic streamfunction (as in section 6c) alone could suffice as a replacement for SLP isobars, keeping in mind that the geostrophic potential function could be important. Boundary layer winds are already a part of model output packages in the NWS, and the effects of the total geostrophic wind are reflected in these winds by the model. Breaking a habit of 100 years duration won't be easy, but the attempt should be made.

The methods used herein can be applied to upper air data in a hybrid sigma-isobaric system. Indeed, this would be necessary because 850 and 700 mb charts also have reduction problems in some areas of the globe. Sangster (1984) has already made some inroads into this realm, and the results are encouraging.

Acknowledgments. The author would like to express gratitude to Dr. Joseph T. Schaefer for helpful comments on the manuscript. Michael D. Manker provided much assistance in the form of computer programming. The National Meteorological Center version of the program was written by Robert J. van Haaren and Peter Henrichsen to whom the author is indebted. The computer facilities of the National Severe Storms Forecast Center were used extensively in the research phase of this project. Many drafts of this paper were expertly prepared by Beverly D. Lambert, Frances M. Curnow and Dorothy L. Babich.

APPENDIX

Obtaining D Values

The data used in these studies came from hourly aviation weather reports for stations in the United States and Canada. Altimeter settings, temperatures, dewpoint temperatures, and sea level pressures were the variables used.

The method of obtaining D values at the smoothed reference terrain will be described here. An empirical formula derived by least-squares curve fitting methods was used to convert altimeter settings to D_{st} (D values at the station levels). This was

$$D_{st} = 281.7(A_s - 29.92) - 4.49(A_s - 29.92)^2. \quad \text{(A1)}$$

Here D_{st} is in meters and A_s (altimeter setting) is in inches Hg. This is sufficiently accurate for the use made herein; a more accurate conversion could be made by using the properties of the standard atmosphere.

We assumed that the mean virtual temperature (T^*) in the column between the station elevation and the smoothed terrain was equal to the virtual temperature at the station (T^*_{st}). From (2) we may write approximately

$$\frac{\partial D}{\partial Z} = \frac{\overline{S^*}}{1+\overline{S^*}} = \frac{\overline{T^*} - \overline{T_p}}{\overline{T^*}} \quad \text{(A2)}$$

Then we may write

$$D_{sm} = D_{st} + (Z_{sm} - Z_{st})\left(1 - \frac{\overline{T_p}}{T^*_{st}}\right) \quad \text{(A3)}$$

where D_{sm} is the D value at the smoothed terrain, and Z_{sm} and Z_{st} are the geopotential heights of the smoothed terrain and the station, respectively.

Now from the definition of the standard atmosphere

$$T_p = a - bZ_p, \quad \text{(A4)}$$

where a = 288 K and b = 0.0065°C m^{-1}.

From (A4) we can say that

$$\bar{T}_p = a - \frac{1}{2}b(Z_{\text{pst}} + Z_{\text{psm}}) = a - \frac{1}{2}b(Z_{\text{pst}} + Z_{sm} - D_{sm}), \tag{A5}$$

where Z_{pst} and Z_{psm} are the pressure altitudes at the station and smoothed terrain.

From (A3) and (A5) we may write

$$D_{sm} = D_{st} + (Z_{sm} - Z_{st})\left[1 - \frac{a - \frac{1}{2}b(Z_{\text{pst}} + Z_{sm})}{T^*_{st}} - \frac{\frac{1}{2}bD_{sm}}{T^*_{st}}\right]. \tag{A6}$$

Finally (A6) gives

$$D_{sm} = \frac{D_{st} + (Z_{sm} - Z_{st})\left[1 - \dfrac{a - \frac{1}{2}b(Z_{\text{pst}} + Z_{sm})}{T^*_{st}}\right]}{1 + \dfrac{b(Z_{sm} - Z_{st})}{2T^*_{st}}}. \tag{A7}$$

REFERENCES

Bellamy, J. C., 1945: The use of pressure altitude and altimeter corrections in meteorology. *J. Meteor.*, **2**, 1–79.

Blackadar, A. K., 1957: Boundary layer wind maxima and their significance for the growth of nocturnal inversions. *Bull. Amer. Meteor. Soc.*, **38**, 283–290.

Bonner, W. D., 1968: Climatology of the low level jet. *Mon. Wea. Rev.*, **96**, 833–850.

——, and J. Paegle, 1970: Diurnal variations in boundary layer winds over the south-central United States in summer. *Mon. Wea. Rev.*, **98**, 735–744.

Cressman, G. P., 1959: An operational objective analysis system. *Mon. Wea. Rev.*, **87**, 367–374.

Ferrel, W., 1886: On reduction of barometric pressure to sea level and standard gravity. *Annual Report of the Chief Signal Officer of the Army, 1886*, Washington, D.C., 1887, Appendix 23.

Harrison, L. P., 1957: Report on the problem of "Reduction of Pressure." Report of the Working Group on Barometry to the World Meteorological Organization, Commission for Instruments and Methods of Observation (CIMO-II), Paris, 118 pp. [Available from World Meteor. Org., Geneva, Switzerland.]

——, 1963: Manual of Barometry (WBAN). U.S. Govt. Printing Office, Washington, DC. [Available from NOAA/National Weather Service, Washington, DC 20233.]

——, 1970: Reduction of surface pressure to functions useful in analysis and forecasting. *Meteor. Monogr.*, No. 33, Amer. Meteor. Soc., 121–136.

Magor, B. W., 1958: A meso-low associated with a severe storm. *Mon. Wea. Rev.*, **86**, 81–90.

Phillips, N. A., 1957: A coordinate system having some special advantages for numerical forecasting. *J. Meteor.*, **14**, 184–185.

Quiroz, R. S., 1984: The climate of the 1983/84 winter—a season of strong blocking and severe cold in North America. *Mon. Wea. Rev.*, **112**, 1894–1912.

Sangster, W. E., 1960: A method of representing the horizontal pressure force without reduction of station pressures to sea level. *J. Meteor.*, **17**, 166–176.

——, 1967: Diurnal surface geostrophic wind variations over the Great Plains. *Preprints, Fifth Conf. on Severe Local Storms*, St. Louis, MO, 146–153. Amer. Meteor. Soc.

——, 1979: Warm season nocturnal quantitative precipitation forecasting for eastern Kansas using the surface geostrophic wind chart. NOAA Tech. Memo. NWS CR-64. NOAA, 44 pp. [Available from National Weather Service, Room 1836, 601 E. 12th Street, Kansas City, MO 64106.]

——, 1984: A hybrid sigma coordinate system as applied to the problem of nocturnal thunderstorm forecasting. *Preprints, Tenth Conf. on Weather Forecasting and Analysis*, Clearwater Beach, FL, Amer. Meteor. Soc., 467–473.

Shuman, F. G., 1957: On the problem of comparing station pressures at varying elevations. Joint Numerical Weather Prediction Unit Office Note No. 7 [Available from National Meteorological Center, National Oceanic and Atmospheric Administration, Washington, DC 20233.]